Time-Resolved Analysis of High-Power-Laser Produced Plasma Expansion in Vacuum

A.Aliverdiev[1,2,5], D.Batani[2], V. Malka[3], T.Vinci[2,4], M.Koenig[4], A.Benuzzi-Mounaix[4] , R.Dezulian[2]

[1] *Institute of Physics of Daghestan Scientific Center of Russian Academy of the Science, 367003, Russia, Daghestan, Makhachkala, 94 Yaragskogo Street, e-mail: aliverdi@frascati.enea.it*
[2] *Dipartimento di Fisica "G. Occhialini", Università degli Studi di Milano-Bicocca, e-mail: batani@mib.infn.it*
[3] *Laboratoire d'Optique Appliquee, UMR CNRS - ENSTA - Ecole Polytechnique, Palaiseau, France*
[4] *Laboratore pour l'Utilisation des Lasers Intenses (LULI), UMR, 7605, CNRS CEA - Université Paris VI - Ecole Polytechnique, 91128 Palaiseau Cedex, France*
[5] *International Humanitarian and Technical Academy, Russia, Daghestan, Makhachkala, 4 Komarova Street*

Abstract. Here we consider the results of an experimental investigation of the temporal evolution of plasmas produced by high power laser irradiation of various types of target materials. The experiment was performed at the LULI Laboratory (Ecole Polytechnique, Paris). We have developed a method to analyze time-resolved streak-camera images and analyzed a number of results obtained with various materials.

INTRODUCTION

The aim of this work is to analyze the process of plasma generation and expansion by high power laser irradiation of different materials, in order to find the temporal-spatial distribution of electron plasma density, to find the temporal and spatial profiles of characteristic velocities of plasma expansion and to analyze these behaviors vs. the atomic number Z and/or the laser energy.

The investigation of hydrodynamics expansion of laser-produced plasmas (in the intensity range $I \approx 10^{14}$ W/cm^3) is of fundamental importance for several physics areas such as inertial confinement fusion. Although several theoretical models of plasma expansion were developed already in the 70's and in the 80's [1-3] and many experiments have studied this aspect, still there are not many "clean" experimental results. Indeed most experiments are influenced by 2D effects in the hydro expansion of the plasma, which arise as a consequence of the small focal spots, which were needed to produce the relatively high laser intensity of interest in these experiments.

In recent years, several techniques have been introduced which allow the production of "flat-top" intensity profiles. Hence one fundamental experimental parameter, the laser intensity on target, is clearly defined, which is not the case with the usual Gaussian-like intensity distribution or, even worse, with focal spots affected by laser hot spots. This allows a well-characterized parametric study of plasma expansion. Also, 2D effects in plasma expansion are strongly reduced, producing a situation much closer to that described by 1D theoretical models. One of such technique is that of Phase Zone Plates (PZP [4]) which appeared in recent years, as an useful investigation tool, and which was also used in our experiment.

EXPERIMENTAL SET UP

The experimental set up includes a Nd:glass high power laser system with typical intensity of 10^{14} W/cm^3 and duration 600 ps, a probe beam (Nd:YAG converted to 2ω) coupled to an interferometer and to a streak-camera with

CP762, *Rarefied Gas Dynamics: 24th International Symposium,* edited by M. Capitelli
© 2005 American Institute of Physics 0-7354-0247-7/05/$22.50

Report Documentation Page

Form Approved
OMB No. 0704-0188

Public reporting burden for the collection of information is estimated to average 1 hour per response, including the time for reviewing instructions, searching existing data sources, gathering and maintaining the data needed, and completing and reviewing the collection of information. Send comments regarding this burden estimate or any other aspect of this collection of information, including suggestions for reducing this burden, to Washington Headquarters Services, Directorate for Information Operations and Reports, 1215 Jefferson Davis Highway, Suite 1204, Arlington VA 22202-4302. Respondents should be aware that notwithstanding any other provision of law, no person shall be subject to a penalty for failing to comply with a collection of information if it does not display a currently valid OMB control number.

1. REPORT DATE	2. REPORT TYPE	3. DATES COVERED
13 JUL 2005	**N/A**	**-**

4. TITLE AND SUBTITLE	5a. CONTRACT NUMBER
Time-Resolved Analysis of High-Power-Laser Produced Plasma Expansion in Vacuum	5b. GRANT NUMBER
	5c. PROGRAM ELEMENT NUMBER
6. AUTHOR(S)	5d. PROJECT NUMBER
	5e. TASK NUMBER
	5f. WORK UNIT NUMBER
7. PERFORMING ORGANIZATION NAME(S) AND ADDRESS(ES) **Institute of Physics of Daghestan Scientific Center of Russian Academy of the Science, 367003, Russia, Daghestan, Makhachkala, 94 Yaragskogo Street,**	8. PERFORMING ORGANIZATION REPORT NUMBER
9. SPONSORING/MONITORING AGENCY NAME(S) AND ADDRESS(ES)	10. SPONSOR/MONITOR'S ACRONYM(S)
	11. SPONSOR/MONITOR'S REPORT NUMBER(S)

12. DISTRIBUTION/AVAILABILITY STATEMENT
Approved for public release, distribution unlimited

13. SUPPLEMENTARY NOTES
See also ADM001792, International Symposium on Rarefied Gas Dynamics (24th) Held in Monopoli (Bari), Italy on 10-16 July 2004.

14. ABSTRACT

15. SUBJECT TERMS

16. SECURITY CLASSIFICATION OF:			17. LIMITATION OF ABSTRACT	18. NUMBER OF PAGES	19a. NAME OF RESPONSIBLE PERSON
a. REPORT **unclassified**	b. ABSTRACT **unclassified**	c. THIS PAGE **unclassified**	**UU**	**6**	

ps resolution. The diagnostic system allows the evolution of the plasma density profile to be measured as a function of time. Different targets (CH, Al, Au) have were in the experiment, with different radiative properties. In particular plasma expansion with Au targets should be strongly influenced by radiation (XUV) transport [5], while, in the case of CH targets, energy transport should be determined by electrons only. Such phenomena are a key problem in the physics of Inertial Confinement Fusion (ICF) driven by lasers.

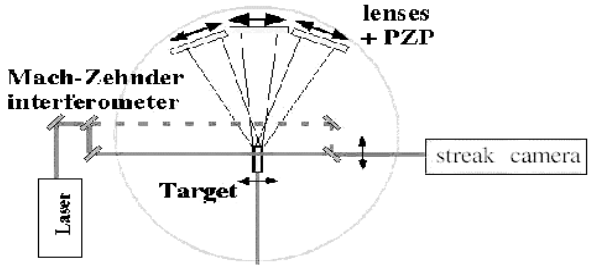

FIGURE 1. Typical experimental set-up used at LULI

Phase Zone Plates (PZP) were used to smooth the laser beam (remove large-scale hot spots) and produce a flat-top irradiation profile, reducing 2D in plasma expansion [4]. The experimental set-up is shown in fig. 1. Fig. 2 shows typical experimental streak-camera images: a) CH and b) Al targets accordantly. The total image dimensions are 375 μm (horizontal scale) and (1.065 ns vertical scale).

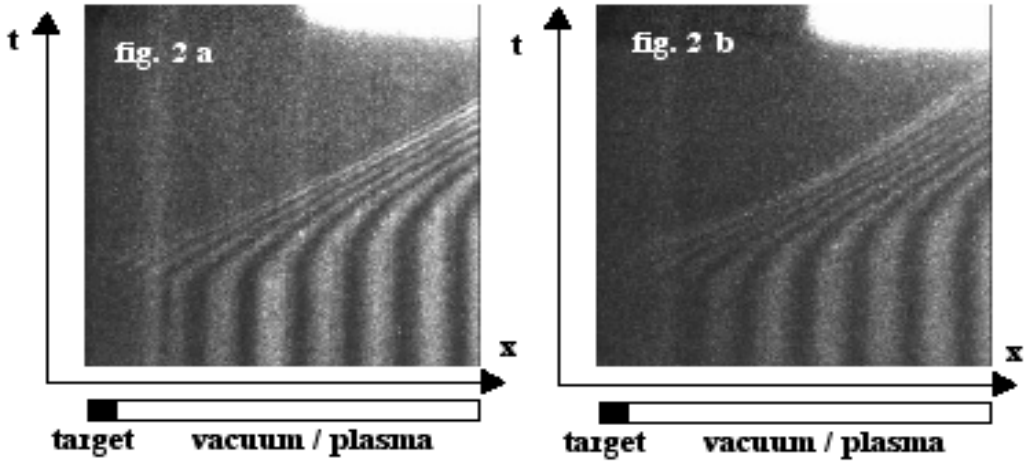

FIGURE 2. Typical interferograms recorded with the streak camera: a) CH and b) Al targets. The total image dimensions are 375 μm (horizontal scale) and (1.065 ns vertical scale).

DETERMINATION OF PLASMA DENSITY

Here we introduce the method used for the analysis of interferometric images, like those presented in fig. 2. The phase shift in a point x of the interferometric picture from classical optics is $\Delta\Phi_a(x) = 2\pi\alpha x / \lambda$, where α is the angle

between the probe and reference beams the in interferometer; and λ the wavelength of the laser beam. The plasma-induced phase shift is $\Delta\phi_{plasma}(x,t) = \frac{2\pi d}{\lambda}\left(1 - \sqrt{1 - \frac{N_e(x,t)}{n_c}}\right)$, where N_e is the density of free electrons, $n_c = \frac{4\pi^2 c^2 \varepsilon_0 m_e}{\lambda^2 e^2}$, the critical density, λ the laser wavelength. Here d is the transversal dimension of the plasma (along probe beam, i.e. perpendicularly to x). In this preliminary analysis, we have taken d = 400 μm, corresponding to the FWHM of the laser focal spot created by the PZPs. Therefore the density can be obtained from the phase shift as: $N_e = n_c\left(1 - \left(1 - \frac{\Delta\phi_{plasma}\lambda}{2\pi d}\right)^2\right)$.In the limiting case $N_e << n_c$, we get $N_e \approx \Delta N_e\, i$, where $\Delta N_e = n_c\, \lambda\, /d$, and where i is the number of π-phase shifts. Hence, every phase shift of π along the temporal axis corresponds to a density jump $\Delta N_e = n_c\left(\left(1 - \frac{\Delta\phi_{plasma0}\lambda}{2\pi d}\right)^2 - \left(1 - \frac{(\Delta\phi_{plasma0} + \pi)\lambda}{2\pi d}\right)^2\right)$in the general case, or $\Delta N_e = n_c\, \lambda\, /d$, in the case $N_e << n_c$.

In the following step of the analysis, we consider the points on the x-axis (spatial dimension), which initially, i.e. before plasma production, correspond to maxima and minima of the interferograms, and we follow here the time evolution of the density N_e in steps of ΔN_e.

For the analysis of the interferograms we have applied a technique of averaging with time shifts, which is similar to the application of the direct Radon transformation, which was discussed in [6].

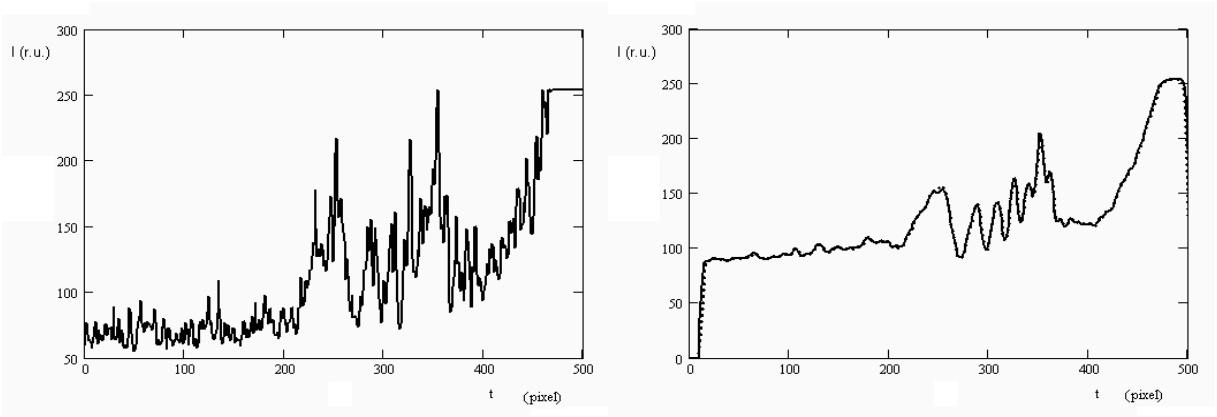

FIGURE 3 (a). time-dependence of intensity in the streak-camera image in fig. 2a, for x_0=481 pixels; **(b).** time-dependence of intensity in the streak-camera image in fig. 2a, for x_0=481 after time-shift averaging in the spatial interval ±20 pixel. The dotted line corresponds to characteristic velocity 1.6, the solid line to 1.8. Finally a Gauss-filter by t as been applied

ANALYSIS OF INTERFEROMETRICAL IMAGES

For the analysis of experimental interferograms, we have attempted to consider a precise numerical method based on averaging with shift on the time axis.

Indeed, if consider ione interferogram, as in fig. 2, and we plot the intensity corresponding to one given position x_0 (vertical densitometry), the presence of a very strong noise (fig. 3 (a)) can result either in neglecting or shifting of real extremes of phase shift, or in the appearance of false extremes. But on the other hand, averaging of several of such densitometries on a small interval Δx_0, centred around x_0, does not give good results, because it smoothes the picture.

In alternative, the averaging with time shifts, with a characteristic velocity more or less correspondent to real velocity, gives a good resolution and a good contrast in the obtained densitometry.

Fig. 3 (a) and (b) give the illustration of the method for the precise determination of extremes in the interferometric streak-camera image, shown in the fig. 2 (a), where x_0=481 pixels, corresponding to the first minimum from the right. The horizontal time scale is also in pixels. The real scale is 512 / 512 pixels for 375 μm / 1065 ps. The vertical scale, giving the intensity on the streak-camera image, is in arbitrary units. How we can see from fig. 3 (b), the differences between locations of extremes for a quite wide range of characteristic time-shift velocities are not more than 1 pixel (the principle limit), showing that our results are quite reliable.

RESULTS AND DISCUSSION

Let us turn back to fig. 2. For the each fixed x, we find 3 zones: (i) the first, where the signal is only modulated in x and independent from t (vertical interference fringes), (ii) the second one, where the signal significantly depends on t (inclined interference fringes), and (iii) third one, practically uniform where the interference fringes disappear. The first, up to a time $t_0(x)$, correspond to the situation without any plasma. At the time t_0, the first plasma reaches the point x (or at least a plasma with a density sufficient to produce a measurable phase shift). The second zone ends at the time t_{cr}, at which the plasma density overcomes some critical value, so that the probe beam is refracted away from the collecting optics. After t_{cr}, of course the fringes disappear and it becomes impossible to determine the plasma density. So, the zone which we can investigate is limited by the curves $t_0(x)$ and $t_{cr}(x)$, which separate the region of non-zero and non-overcome electron density.

Within this zone, for each fixed x, we can further distinguish 3 regions: (i) first growth, (ii) constant behaviour, and (iii) final fast growth. For a better analysis of such behaviour, we consider the dependence of the growth velocity dN_e/dt from N_e (fig. 4 shows such dependence for x=303 μm).

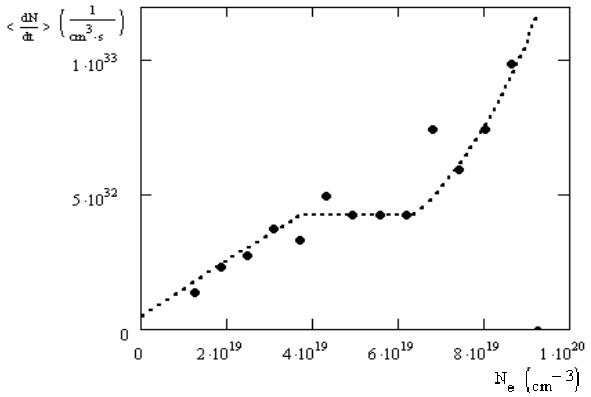

FIGURE 4. Velocity growth of electron density, vs. electron density, for x=303 μm, as deduced from fig. 1 a.

Starting from the typical dependence shown in fig. 4, we can write:

$$dN_e/dt = (\Delta N_e / \Delta t_{||})\, f(N_e, x) \tag{1}$$

where ΔN_e and $\Delta t_{||}$ corresponds to the previously introduced density jump inducing a π-phase shift and to the time difference between value of N_e with phase shift π in the interferometric picture in the second (constant) region. Solving this differential equation we can find the formula for the time $t(N_e, x)$, at which an electron density N_e is

realized in the point x. This is $t(N_e,x) = t_0(x) + \frac{\Delta t_{\|}}{\Delta N_e}\int_0^{N_e}\frac{dN_e}{f(N_e,x)}$ where $t_0(x)$ is the time, where the first plasma reaches the point x, as before. For the function $f(N_e,x)$ we could find an empirical equation:

$$f(N_e,x) = \begin{cases} A(x) + (1-A(x))\cdot(N_e/N_{cr1}) & , \quad N_e < N_{cr1} \\ 1 & , \quad N_{cr1} < N_e < N_{cr2}(x) \\ \exp\left(B(x)\cdot\left((N_e/N_{cr2}(x))-1\right)\right) & , \quad N_e > N_{cr2}(x) \end{cases} \tag{2}$$

where $A(x)$ is an empirical linear function characterizing of the growth of N_e in the first region; $B(x) = \ln(1/A(x))$, and N_{cr1} and N_{cr2} are the electron densities corresponding to the beginning and the end of the constant phase in fig. 4. It is necessary to remark that if formally $N_{cr1}>N_{cr2}$ the function *f(x)* has no constant region. We can finally find the dependence of N_e from t and x. If the function function *f(x)* has a constant region, this is:

$$N_e(t,x) = \begin{cases} \frac{N_{cr1}\cdot A(x)}{1-A(x)}\cdot\left(\exp\left(\frac{(t-t_0(x))\cdot(1-A(x))\cdot\Delta N_e}{N_{cr1}\cdot\Delta t_{\|}}\right)-1\right) & , \quad t < t_{cr1}(x) \\ N_{cr1} + (\Delta N_e/\Delta t_{\|})\cdot(t-t_{cr1}(x)) & , \quad t_{cr1}(x) < t < t_{cr2}(x) \\ N_{cr2}(x)\cdot\left(B(x) - \ln\left(\exp(B(x)-1) - \frac{(t-t_{cr2}(x))\cdot N_{cr2}(x)}{\Delta t_{\|}\cdot\Delta N_e}\right)\right) & , \quad t_{cr2}(x) < t \end{cases} \tag{3}$$

where $t_{cr1}(x) = t_0(x) + \frac{\Delta t_{\|} N_{cr1} B(x)}{\Delta N_e\cdot(1-A(x))}$ $\qquad$ $t_{cr2}(x) = t_{cr1}(x) + \Delta t_{\|}\cdot\frac{N_{cr2}(x)-N_{cr1}}{\Delta N_e}$

while, if the function *f(x)* has no constant region

$$N_e(t,x) = \begin{cases} \frac{N_{cr1}\cdot A(x)}{1-A(x)}\cdot\left(\exp\left(\frac{(t-t_0(x))\cdot(1-A(x))\cdot\Delta N_e}{N_{cr1}\cdot\Delta t_{\|}}\right)-1\right) & , \quad t < t_{cr2}(x) \\ N_{cr2}(x)\cdot\left(B(x) - \ln\left(\exp(B(x)-1) - \frac{(t-t_{cr2}(x))\cdot N_{cr2}(x)}{\Delta t_{\|}\cdot\Delta N_e}\right)\right) & , \quad t_{cr2}(x) < t \end{cases} \tag{4}$$

where $t_{cr2}(x) = t_0(x) + \Delta t_{\|}\cdot\frac{N_{cr1}(x)}{1-A(x)}\cdot\ln\left(1+\frac{N_{cr2}(x)\cdot(1-A(x))}{A(x)\cdot N_{cr1}(x)}\right)$. From our preliminary analysis, we can conclude that N_{cr1} is more or less independent on x, N_{cr2} strongly depends on the point x, $\Delta t_{||}$ is practically independent from x for the CH target.

From the calculated values of $N_e(t,x)$ we can reconstruct the interferograms. We can observe (see fig. 5, which presents the comparison between reconstructed interferograms (stripes without noise) and experimental ones (stripes with noise) for the cases presented in fig. 1, CH (left) and Al (right) targets.) how these correspond very well to the experimental interferograms for *all* values of x and t.

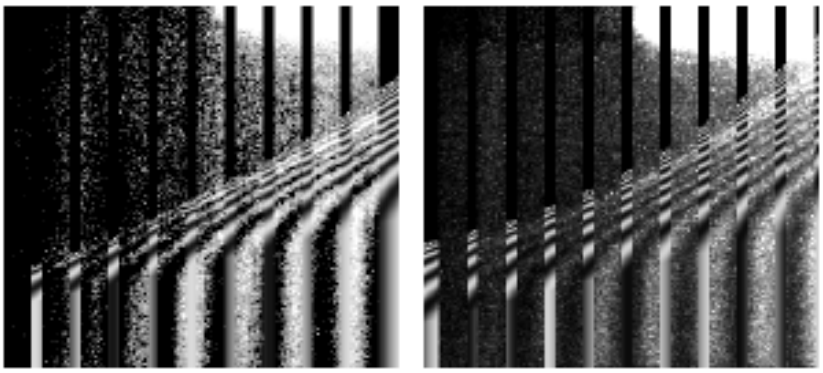

FIGURE 5. Comparison between reconstructed interferograms (stripes without noise) and experimental ones for the cases presented in fig. 1, CH (left) and Al (right) targets.

CONCLUSION

In conclusion, we have found a reasonable way to analyze the interferograms and reconstruct them, and we have found some phenomenological behavior. It should be stressed that the values of N_e, which we calculated, are **NOT** the real values of electron density. Indeed they have been calculated by assuming a plasma transversal size d = 400 μm (equal to the FWHM size of the focal spot) and keeping it constant in time. Hence in reality the variation evidenced in fig. 4 rather corresponds to the evolution of the line integral $\int N_e(x,y,t)dy$ (y being the coordinate along the probe beam, perpendicular to x) which we assumed to be $\approx(N_e\ d)$. A more proper analysis will need to consider the time evolution of the plasma transversal size, through a 2D hydrodynamics modeling.

ACKNOWLEDGMENTS

The authors warmly acknowledge the help of the LULI technical staff for the realization of this experiment. The work of A.A. was supported by a fellowship of the Cariplo Foundation organized by the Landau Network-Centro Volta.

REFERENCES

1. C.E. Max, et al., Phys. Fluids, **23**, 1620 (1980).

2. W.M.Manheimer, D.G.Colombant, J.H.Gardner "Steady-state planar ablative flow", Phys. Fluids **25**, 1644 (1982)

3. P.Mora "Theoretical model of absorption of laser light by a plasma", Phys. Fluids **25** (6) (1982)

4. M. Koenig, et al., *Phys. Rev. E* **5**0, R3314 (1994)

5. R. Sigel, et al., Physical Review Letters **65**, 587 (1990); N.Kaiser, J. Meyer-ter-Vehn, R. Sigel, Physics of Fluids B, **1**, 1747 (1989)

6. A.A.Aliverdiev. Proc. of. 25th Int. Conf. on Phenomena in Ionized Gases, Nagoya, Japan, 2001, **4**, pp. 59-60